



Drone remote sensing of wheat N using hyperspectral sensor and machine learning

Rabi N. Sahoo¹ · R. G. Rejith¹ · Shalini Gakhar¹ · Rajeev Ranjan¹ · Mahesh C. Meena² · Abir Dey² · Joydeep Mukherjee¹ · Rajkumar Dhakar¹ · Abhishek Meena¹ · Anchal Daas³ · Subhash Babu³ · Pravin K. Upadhyay³ · Kapila Sekhawat³ · Sudhir Kumar⁴ · Mahesh Kumar⁴ · Viswanathan Chinnusamy⁴ · Manoj Khanna⁵

Accepted: 23 October 2023 / Published online: 8 November 2023

© The Author(s), under exclusive licence to Springer Science+Business Media, LLC, part of Springer Nature 2023

Abstract

Plant nitrogen (N) is one of the key factors for its growth and yield. Timely assessment of plant N at a spatio-temporal scale enables its precision management in the field scale with better N use efficiency. Airborne imaging spectroscopy is a potential technique for non-invasive near real-time rapid assessment of plant N on a field scale. The present study attempted to assess plant N in a wheat field with three different irrigation levels (I_1 – I_3) along with five nitrogen treatments (N_0 – N_4) using a UAV hyperspectral imager with a spectral range of 400 to 1000 nm. A total of 61 vegetative indices were evaluated to find suitable indices for estimating plant N. A hybrid method of R-Square (R^2) and Variable Importance Projection (VIP) followed by Variance Inflation Factor was used to limit the best suitable N-sensitive 13 spectral indices. The selected indices were used as feature vectors in the Artificial Neural Network algorithm to model and generate a spatial map of plant N in the experimental wheat field. The model resulted in R^2 values of 0.97, 0.84, and 0.86 for training, validation, and testing respectively for plant N assessment.

Keywords UAV · Leaf nitrogen assessment · Vegetative indices · Machine learning · ANN

Introduction

High productivity with enhanced nutrient-use efficiency is one of the important desirable agronomic, economic, and environmental goals in crop husbandry (Haque, 2006). In most crops, nitrogen (N) is the most limiting nutrient for crop production (Ågren et al., 2012), and its efficient use is important for economic and ecological sustainability (Mălinaş et al., 2022). Wheat (*Triticum aestivum* L.) is a high N-demanding crop, where insufficient application of it may result in reduced production, whereas excessive fertilization implies wasting resources and an increase in environmental pollution (Good & Beatty, 2011). Nitrogen fertilization of wheat can account for up to 30% of the total production cost and around 50–75% of the N applied to the field is not used by the plant and is lost by leaching into the soil (Baresel et al., 2008; Hirel et al., 2011). Therefore,

Extended author information available on the last page of the article

nitrogen is a key element required for plant growth, and is one of the most important yield-limiting nutrients in crop production in all agroecological regions of the world (Guo et al., 2019; Zhu et al., 2007). Therefore, rapid and accurate detection of the wheat nitrogen status is of great significance for growth diagnosis and precision management to achieve higher yield and better quality while also minimizing adverse environmental impacts (Yang et al., 2019).

At present, the implementation of remote sensing (RS) technology in precision agriculture provides new opportunities for the non-destructive real-time diagnosis of plant nitrogen status (Blekanov et al., 2023; Sahoo et al., 2015) and precision nitrogen management over a large area (Rabatel et al., 2017). Vegetation indices (VIs) derived from multiple spectral bands are now widely used in developing N monitoring models for various crops (Basyouni et al., 2015; Jiang et al., 2020; Ranjan et al., 2012; Xu et al., 2023). This technology contributed to the development of RS-based variable rate N recommendation approaches, which mainly use the remotely sensed crop growth information as the chief attribute of N fertilization (Späti et al., 2021).

Many researchers have attempted to derive the crop biophysical and chemical parameters using (VIs) derived from field spectral measurements (Dehghan-Shoar et al., 2023), and sensors on satellites (Jamali et al., 2023) and unmanned aerial vehicles (UAVs) (Buthelezi et al., 2023). Even though satellite-based multispectral images are useful to aid N management, farmers are still reluctant to adopt RS technologies. Satellite images normally have lower spatial and temporal resolution and, in some areas, they can be distressed by cloud cover during the image acquisition (Hunt et al., 2005). UAVs have tremendous potential for high-resolution requirements for site-specific management of weed control (Anderegg et al., 2023; Esposito et al., 2021; Jurado-Expósito et al., 2021) and N recommendation (Jiang et al., 2023; Maresma et al., 2016).

The advent of hyperspectral UAV sensors with narrow band widths made a breakthrough in crop monitoring by providing an accurate prediction of plant N levels and thereby N stress estimation. Leaf nitrogen content (LNC) of wheat was predicted by using first derivative normalized difference nitrogen index (FD-NDNI) and the first derivative ratio nitrogen vegetation index (FD-SRNI) with the help of random forest (RF) (Liang et al., 2018); the transformed chlorophyll absorption in the reflectance index/optimized soil-adjusted vegetation index (TCARI/OSAVI) on using partial least squares regression (PLSR) and modern machine learning (ML) methods, including artificial neural network (ANN), RF, and support vector machine (SVM) (Wang et al., 2021). Among the various non-parametric modeling algorithms, the RF approach performed best for estimating LNC in winter wheat using modified renormalized difference VI (RDVI) from UAV Multispectral Images (Zheng et al., 2018). Several other researchers also proposed UAV-based multispectral and hyperspectral VIs for LNC prediction in crops using different machine learning approaches (Fu et al., 2022; Jiale Jiang et al., 2019; Li et al., 2018; Liu et al., 2017; Osco et al., 2020; Xu et al., 2023; Zhang et al., 2022).

On account of potential applications of UAV hyperspectral remote sensing in the field of agriculture and the importance of N management practices, the present study emphasizes the performance of various hyperspectral vegetation indices for wheat leaf N estimation. The study conducted involves an exhaustive comparative assessment of the VIs for wheat leaf N assessment and was performed in multiple stages, (1) UAV-based hyperspectral data collection and pre-processing (2) selection of the most significant indices for leaf nitrogen prediction and (3) prediction of leaf N through ANN using selected indices as input.

Dataset

Experimental site and field sampling

An experiment was conducted on the Research Farm of ICAR-Indian Agricultural Research Institute, New Delhi with wheat crop (variety-HD 3059) during the rabi (winter) season 2021-22. The field is situated between $28^{\circ}38'29.99''\text{N}$ to $28^{\circ}38'26.58''\text{N}$ latitudes and $77^{\circ}9'0.99''\text{E}$ to $77^{\circ}9'5.09''\text{E}$ longitudes. The experiment was conducted in a split-plot design with three irrigation types as the main plot: I_1 -soil moisture sensor-based irrigation, I_2 -CWSI-based irrigation, and I_3 -conventional irrigation. Under each irrigation level, there were five levels of nitrogen application i.e., 0, 50, 100, 150, and 200 kg ha^{-1} corresponding to N_0 to N_4 , respectively as sub-plot treatment. As a basal dose, one-third of recommended N and full recommended phosphorus (P) and potassium (K) were applied as urea (46% N), diammonium phosphate (18% N and 46% P_2O_5), and muriate of potash (60% K_2O), respectively. The remaining N was applied later in two equal split doses during the first and second irrigations. There were three replications R_1 , R_2 , and R_3 . The wheat crop was sown on 13th December 2021 and was harvested on 15th April 2022. The size of the sub-plot and main plot were kept as 93.6 m^2 ($7.2 \times 13\text{ m}$) and 468 m^2 ($7.2 \times 65\text{ m}$), respectively. The location map of the study area and its experimental layout is presented in Fig. 1. The study area experiences a

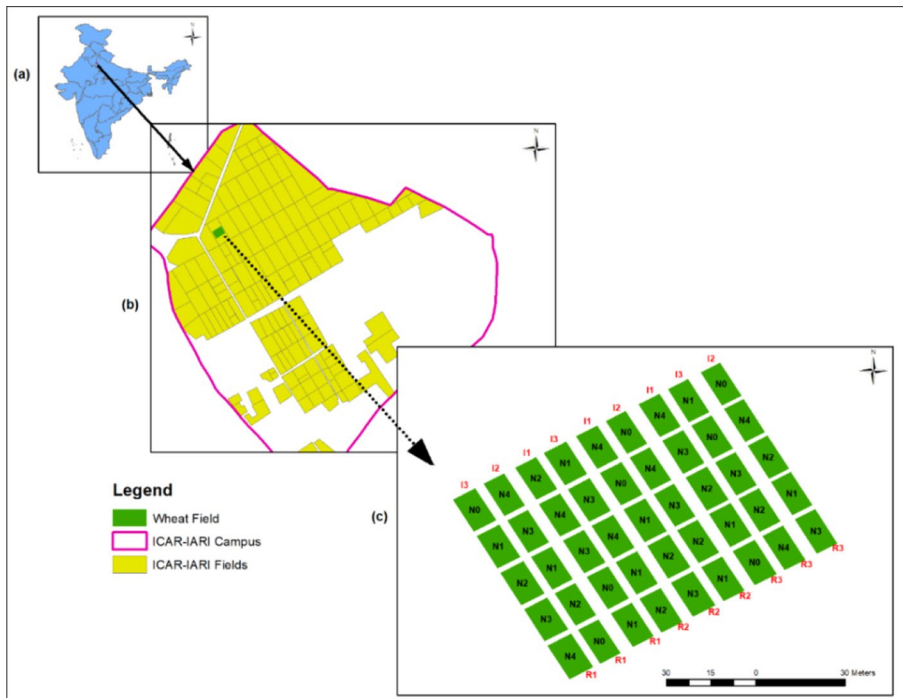


Fig. 1 Study area map showing the Geographic location of the experimental plots with different fertilization treatments. **a, b** The location of the ICAR- IARI campus and experimental wheat plots. **c** Wheat field layout



Fig. 2 **a** Drone with hyperspectral camera facing nadir, **b** image data acquisition in wheat field

Table 1 Major specifications of UAV hyperspectral sensor

Nano-hyperspec hyperspectral sensor		
1.	No. of bands	269
2.	Spectral range	400–1000 nm
3.	Spectral resolution	2.2 nm
4.	frame rate	300 Hz
5.	Spatial resolution	3.4 cm (for current mission)
6.	Signal to Noise	> 15:1 (1000 nm) < 140:1 (550 nm)
7.	Total storage limit	480 GB
8.	Focal Length	4.8 m
9.	Weight	1.2 kg

semi-arid climate with warm long summers lasting from April to August, monsoon in July–September, and mild winter in October. The soil is sandy loam (Typic Haplustepts) having a medium to angular blocky structure and non-calcareous texture. The soil is slightly alkaline with a mean pH of 8.0, mean electric conductivity of 0.25dSm^{-1} and organic carbon of 0.57%. The average nitrogen-phosphorous-potassium (NPK) content of the soil is estimated as 217.1, 52.6, and 508.0 kgha^{-1} , respectively.

Hyperspectral image acquisition using UAV

The hyperspectral images of the wheat crop were captured using a hyperspectral camera (Nano Hyperspec of Headwall Photonics Inc., Bolton, MA, USA) mounted on a hexacopter (Fig. 2). The UAV data acquisition was conducted on 7th February 2022 during day time between 11:00 hrs to 12:00 hrs on a sunny day within a wind speed of $2\text{--}3\text{ ms}^{-1}$, relative humidity ranging between 39–41%, and a temperature of $21\text{ }^{\circ}\text{C}$. The specifications of the imaging sensor used are summarized in Table 1. The flight path planning for the survey has been done using UgCS Mission planning software (UgCS, 2017) which allows the remote monitoring of the flying route, speed of the drone, height above the ground, and overlapping.

Methodology

Preprocessing of hyperspectral image data

The pre-processing of the acquired hyperspectral image data involved (1) conversion of digital numbers (DN) to radiance, (2) calculation of reflectance values, (3) image orthorectification (4) generation of ortho-mosaicked image for analysis (5) spectral smoothing and (6) crop area segmentation.

Raw data conversion

The acquired raw data was converted to radiance followed by reflectance using Headwall SpectralView software version 3.1.4 (Headwall Photonics, Bolton, MA, USA). The dark signal needs to be captured during image data acquisition due to varying sensor characteristics, such as sensor settings and orientation. To obtain an absolute radiometric value from the sensor it has to be calibrated since its signal is subject to influences other than the impinging light. The raw hyperspectral data cubes use the dark reference of the sensor captured pre-flight. The radiance dataset of individual scan lines was processed using the white reference generated using the reflectance data from pixels of calibration tarp placed in the field during flight. The positioning information from Global Navigation Satellite System (GNSS) receivers and Inertial Measurement Unit (IMU) synchronized with data and the Shuttle Radar Topography Mission (SRTM) Digital Elevation Model was used for orthorectification (Santos-Rufo et al., 2020). The geo-rectified hyperspectral data cubes were stitched together and validated by overlaying with Google Earth imagery. The signal noise present in the calibrated image has been removed by applying a Savitzky–Golay (SG) smoothing filter with a second-order polynomial and the frame lengths of 5, available in image processing software ENVI 5.5 (L3 Harris Geospatial, Boulder, CO, USA) (Ge et al., 2019).

Crop area segmentation

The wheat canopy from 45 subplots was extracted using a combined approach of thresholding of hyperspectral normalized difference vegetation index (hNDVI) (Rouse et al., 1974) and spectral angle mapper (SAM) binary masks (Rejith et al., 2020). The threshold for the hNDVI was selected from the histogram representing the frequency of vegetation index values corresponding to all 45 subplots of different N treatments. A threshold value was selected halfway between the vegetation peak and the neighbouring trough. The SAM classification was further carried out using the endmembers spectra computed manually by selecting the pixels of wheat, other vegetation features, and soil. The SAM measures the spectral angle between the endmember spectra and the image spectra in n-dimensional space. Lowering the angle suggests a closer match to reference spectra. The hNDVI mask was later multiplied with SAM binary mask to generate a primary mask image. Then the morphological erosion operator (3×3 matrix of ones) was applied to it to remove the mixed pixels from the canopy edges. Finally, this approach generates a complete mask that was used for concealing the wheat pixels from the neighbouring soil, shadow, and grass pixels in the hyperspectral image dataset. The

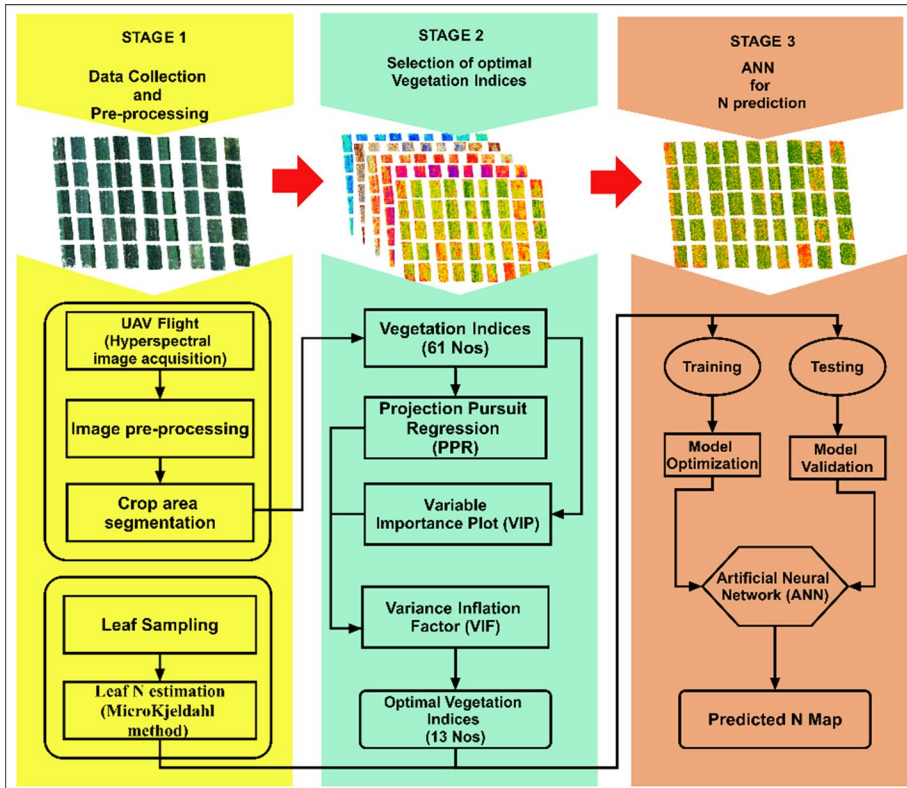


Fig. 3 Flow chart showing the methodology adopted for the study

flow chart showing the proposed methodology adopted for the present study is given in Fig. 3.

Computation of vegetation indices

After an exhaustive review of the literature, a total of 61 vegetation indices (Table 2) were selected for leaf N assessment using imaging spectroscopy (Adak et al., 2021; Chandel et al., 2019; Liang et al., 2018; Pradhan et al., 2013; Ranjan et al., 2012). It is evident from previous studies that, indices-based approaches combined with prediction techniques have yielded optimum results for N assessment. The $NDVI_{Ts}$ constructed by spectral and textural information of UAV multispectral imagery performed well in wheat leaf nitrogen concentration (LNC) monitoring (Fu et al., 2022). Vegetation indices such as NDRE or RERVI composed of near-infrared and red edge bands of UAV—multispectral scanner (UAV-MSS) data showed better results for estimating crop nitrogen status in rice plants (Li et al., 2018). Four representative vegetation indices such as the Visible Atmospherically Resistant Index (VARI), Red edge Chlorophyll Index ($CI_{red-edge}$), Green band Chlorophyll Index (CI_{green}), Modified Normalized Difference Vegetation Index with a blue band (mND_{blue}) were derived from the multi-angular UAV-MSS images for estimating LNC, plant nitrogen

Table 2 List of spectral indices commonly used for the N estimation (R_x = reflectance at λ wavelength)

S. No.	Spectral indices	Formula	Refs.	S. No.	Spectral indices	Formula	Refs.
1	Simple ratio pigment index (SRPI)	R_{430}/R_{680}	Peñuelas et al. (1994)	32	Modified normalized difference vegetation index (mNDVI)	$(R_{800} - R_{680}) / (R_{800} + R_{680} - 2R_{445})$	Sims & Gamon (2002)
2	Simple ratio (SR_900)	R_{900}/R_{680}	Gitelson et al. (1996)	33	Renormalized difference vegetation index (RDVI)	$(R_{800} - R_{670}) / [(R_{800} + R_{670})^{0.5}]$	Roujean & Breon (1995)
3	Pigment-specific simple ratio-a (PSSRa)	R_{800}/R_{680}	Blackburn (1998)	34	Normalized pigment chlorophyll index (NPChI)	$(R_{680} - R_{430}) / (R_{680} + R_{430})$	Peñuelas et al. (1994)
4	Pigment-specific simple ratio-b (PSSRb)	R_{800}/R_{635}	Blackburn (1998)	35	Normalized phaeophytinization index (NPQI)	$(R_{415} - R_{435}) / (R_{415} + R_{435})$	Barnes et al. (1992)
5	Pigment-specific simple ratio-c (PSSRc)	R_{800}/R_{470}	Blackburn (1998)	36	Pigment-specific normalized difference (PSNDa)	$(R_{800} - R_{680}) / (R_{800} + R_{680})$	Blackburn (1998)
6	Buschman and Nagel index (BNI)	R_{550}/R_{800}	Buschmann & Nagel (1993)	37	Pigment-specific normalized difference (PSNDb)	$(R_{800} - R_{635}) / (R_{800} + R_{635})$	Blackburn (1998)
7	Gitelson and Merzlyak index-1 (GMI-1)	R_{750}/R_{550}	Gitelson & Merzlyak (1998)	38	Pigment-specific normalized difference (PSNDc)	$(R_{800} - R_{470}) / (R_{800} + R_{470})$	Blackburn (1998)
8	Gitelson and Merzlyak index-2 (GMI-2)	R_{750}/R_{700}	Gitelson & Merzlyak (1998)	39	Normalized difference chlorophyll index (NDChI)	$(R_{762} - R_{527}) / (R_{762} + R_{527})$	Marshak et al. (2000)
9	Simple ratio ₇₀₅ (SR ₇₀₅)	R_{750}/R_{705}	Gitelson & Merzlyak (1994)	40	Green normalized difference vegetation index (GNDVI)	$(R_{750} - R_{550}) / (R_{750} + R_{550})$	Gitelson et al. (1996)
10	Modified simple ratio ₇₀₅ (mSR ₇₀₅)	$(R_{750} - R_{445}) / (R_{705} - R_{445})$	Sims & Gamon (2002)	41	Green vegetation index (GVI)	$(R_{682} - R_{553}) / (R_{682} + R_{553})$	Kauth and Thomas (1976)

Table 2 (continued)

S. No.	Spectral indices	Formula	Refs.	S. No.	Spectral indices	Formula	Refs.
11	Simple ratio ₅₃₃ (SR ₅₃₃)	R_{533}/R_{565}	Tian et al. (2011)	42	Lichtenthaler indices (Lic1)	$(R_{790} - R_{680}) / (R_{790} + R_{680})$	Lichtenthaler et al. (1996)
12	Modified simple ratio (MSR)	$(R_{800}/R_{670} - 1) / ((R_{800}/R_{670}) + 1)$	Chen (1996)	43	Lichtenthaler indices (Lic2)	R_{440}/R_{690}	Lichtenthaler et al. (1996)
13	Vogelmann red edge index 1 (VREI1)	R_{740}/R_{720}	Vogelmann et al. (1993)	44	Vogelman index c (VOGc)	$(R_{734} - R_{747}) / (R_{715} + R_{720})$	Pablo J. Zarco-Tejada et al. (2001)
14	Vogelman red edge index 2 (VREI2)	$(R_{734} - R_{747}) / (R_{715} + R_{726})$	Vogelmann et al. (1993)	45	Normalized difference red edge (NDRE)	$(R_{790} - R_{720}) / (R_{790} + R_{720})$	Rodriguez et al. (2006)
15	Water band index (WBI)	R_{900}/R_{970}	Penuelas et al. (1993)	46	Modified red edge normalized difference vegetation index (MRENDVI)	$(R_{750} - R_{705}) / (2 \times R_{445})$	Sims & Gamon (2002)
16	Zarco and Miller (ZM)	R_{750}/R_{710}	Pablo J. Zarco-Tejada et al. (2001)	47	Red-edge position (REP)	$700 + [40(R_{670} + R_{780})/2 - R_{700}] / (R_{740} - R_{700})$	Guyot & Baret (1988)
17	Ratio index-half (RI-half)	R_{747}/R_{708}	Gupta et al. (2003)	48	Red normalized difference vegetation index (RNDVI)	$(R_{780} - R_{670}) / (R_{780} + R_{670})$	Raun et al. 2001)
18	Ratio index-1dB (RI-1dB)	R_{735}/R_{720}	Gupta et al. (2003)	49	Photochemical reflectance index (PRI)	$(R_{531} - R_{570}) / (R_{531} + R_{570})$	Garbulsky et al. (2011)
19	Ratio index-2dB (RI-2dB)	R_{738}/R_{720}	Gupta et al. (2003)	50	Plant senescence reflectance index (PSRI)	$(R_{680} - R_{500}) / R_{750}$	Merzlyak et al. (1999)
20	Ratio index-3dB (RI-3dB)	R_{744}/R_{717}	Gupta et al. (2003)	51	Structure insensitive pigment index (SIPi)	$(R_{800} - R_{445}) / (R_{800} - R_{680})$	Penuelas et al. (1995)
21	Red green index (RGI)	R_{690}/R_{550}	Zarco-Tejada et al. (2005)	52	Modified normalized difference ₇₀₅ (mND ₇₀₅)	$(R_{750} - R_{705}) / (R_{750} + 2R_{445})$	Penuelas et al. (1995)

Table 2 (continued)

S. No.	Spectral indices	Formula	Refs.	S. No.	Spectral indices	Formula	Refs.
22	RV11 _(810,560)	R_{810}/R_{560}	Xue et al. (2004)	53	Medium resolution imaging spectrometer (MERIS) terrestrial chlorophyll index (MTCI)	$(R_{750} - R_{710}) / (R_{710} - R_{680})$	Datt (1999)
23	RV12 _(950,660)	R_{950}/R_{660}	Zhu et al. (2008)	54	NVI	$(R_{777} - R_{447}) / R_{673}$	Dash & Curran (2004)
24	RV13 _(810,660)	R_{810}/R_{660}	Zhu et al. (2008)	55	Soil adjusted vegetation index (SAVI)	$[(R_{800} - R_{670}) / (R_{800} + R_{670} + 0.5)] * (1 + 0.5)$	Gupta et al. (2001)
25	Carter index 1 (Ct1)	R_{760}/R_{695}	Carter (1994); Garbulsky et al. (2011)	56	Modified soil-adjusted vegetation index (MSAVI)	$0.5 \times \{2R_{800} + 1 - [(2R_{800} + 1)^2 - 8(R_{800} - R_{670})^{0.5}]\}$	Qi et al. (1994)
26	Curvature index (CI)	$R_{675} (R_{690}/R_{683}^2)$	Zarco-Tejada et al. (2005)	57	OSAVI	$(1 + 0.16) (R_{800} - R_{670}) / (R_{800} + R_{670} + 0.16)$	Rondeaux et al. (1996)
27	Curvature index 1 (CI1)	R_{440}/R_{690}	Zarco-Tejada et al. (2005)	58	V1opt	$(1 + 0.45) ((R_{800})^2 + 1) / (R_{670} + 0.45)$	Rondeaux et al. (1996)
28	Green index (GI)	R_{554}/R_{677}	Zarco-Tejada et al. (2005)	59	Triangular vegetation index (TVI)	$0.5 [1.20 (R_{750} - R_{550}) - 200 (R_{670} - R_{550})]$	Broge & Leblanc (2001)
29	Hyperspectral normalized difference vegetation index (hNDVI)	$(R_{900} - R_{685}) / (R_{900} + R_{685})$	Rouse et al. (1974)	60	Modified triangular vegetation index (MTVI)	$1.2 [1.2(R_{800} - R_{550}) - 2.5 (R_{670} - R_{550})]$	Haboudane et al. (2004)
30	Normalized difference705 (ND ₇₀₅)	$(R_{750} - R_{705}) / (R_{750} + R_{705})$	Gitelson & Merzlyak (1994)	61	Second modified triangular vegetation index (MTVI2)	$[1.5 (1.2 \times (R_{800} - R_{550}) - 2.5 (R_{670} - R_{550})) / ((2(R_{800} + 1)^2 - (6R_{800} - 5(R_{670}^{0.5})))^{0.5}) - 0.5]^{0.5}$	Haboudane et al. (2004)
31	NDVI (573, 440)	$(R_{573} - R_{440}) / (R_{573} + R_{440})$	Datt (1999)				

concentration (PNC), leaf nitrogen accumulation (LNA), and plant nitrogen accumulation (PNA) of wheat canopies (Lu et al., 2019).

To compare the performance of different spectral indices for leaf N content at various N fertilizer treatments, twenty-five points were randomly selected within each subplot by excluding an inner buffer distance of 1m from the borders. This approach facilitates the exact measurements of crops and avoids the areas of bare soil without crops (Maresma et al., 2016). At last, the mean of the values extracted at each point within a subplot was used to determine the best vegetation index/es to predict LNC. Three sets of top-most leaf samples were collected from each plot for N determination and their mean was taken. The N concentration of leaf samples was estimated using the Micro-Kjeldahl method (Guebel et al., 1991; Ranjan et al., 2012).

Selection of suitable indices

Selection of optimal spectral bands through R^2

The R^2 value for all 61 derived indices was calculated for the growth stage under study. R^2 value equal to or higher than 0.7 was considered as optimum for N assessment. In this approach, an index-by-index linear correlation matrix was computed to interpret redundant information. Further, Pearson correlation coefficient (R) values have been squared (R^2) to remove inverse correlation.

Selection of optimal spectral bands through PPR-VIP statistics

Projection pursuit regression (PPR) is a multivariate statistical technique comprising of three-layered architecture with input, hidden, and output layers. Unlike the linear regression approach, which assumes a direct linear combination of the predictor variables accumulating the cost of inaccurate predictions; PPR is a non-parametric regression algorithm. The algorithm helps in finding the most suitable model for prediction problems. Projection ‘directions’ or ‘strengths’ between input and hidden neurons; hidden and output neurons and the activation function are calculated by minimizing the error using least square criteria. The mathematical formulation of the model is given by Eq. 1.

$$L = \sum_{i=1}^q [y_i - \sum_{k=1}^m \beta_{ik} f_k(\alpha_k^T x)]^2 \quad (1)$$

where, $\alpha_k^T = [\alpha_{k1}, \dots, \alpha_{kp}]$ is the projection directions given by weights between the input and the hidden layers; $\beta_k = [\beta_{1k}, \dots, \beta_{qk}]$ is the projection directions given by weights between the hidden layers and the output layer; f_k is the activation function; y_i is the response variable which is modelled as a weighted linear combination of the activation function. PPR learns layer by layer and calculates the weights by least square estimation.

Variable importance Projection (VIP) is a statistical technique for synthesizing the contribution of predictors and response variables. This measure is highly dependent on the accuracy and importance of the fitted model (here, PPR). It summarizes the contribution of a variable to the model. The indices with the highest VIP values (centers of the peaks observed) have been selected by keeping the threshold value as 0.5. The equation is given as:

$$\sqrt{n \frac{\sum_{j=1}^a b_j^2 t_j^T t_j \left(\frac{w_{kj}}{\|w_j\|} \right)^2}{\sum_{j=1}^a b_j^2 t_j^T t_j}} \tag{2}$$

where b is the regression coefficient, w_j is the weight vector, t_j is the score vector for the k^{th} element.

Selection of optimal spectral bands through VIF statistics

The Variance Inflation Factor (VIF) helps in measuring the multicollinearity in regression algorithms. It quantifies the inflation of variance of estimated coefficients. Inflation factors were calculated by regressing the predictor with every other predictor variable considered for the model followed by the computation of R-squared values. The VIF for the i^{th} predictor is given by:

$$VIF = \frac{1}{1 - R_i^2} \tag{3}$$

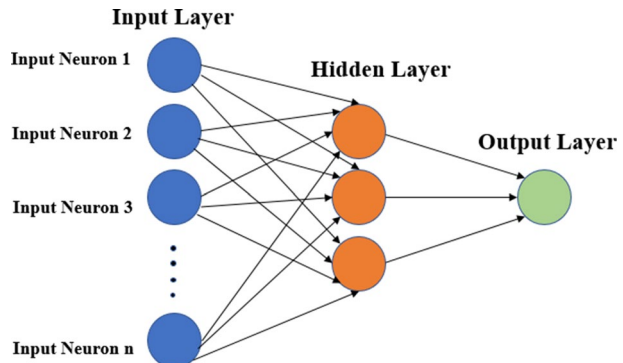
where R_i^2 is the r-square value obtained.

Artificial neural network (ANN)

ANN mimics the functionality of a human brain where neurons work as the most fundamental unit to perform complex tasks. It is a three-layered architecture including input, hidden, and output layers, along with an activation function that ignites the most significant neuron as the output (Fig. 4). The fully connected structure is managed by weights from the input to the hidden layer followed by the hidden to the output layer (Fig. 5). ANN being a machine learning measure, can learn from the data and predict accordingly. The data traverses through the hidden layer which transforms the data into a usable form to generate the result, that is it helps in extracting useful information from raw data by generalizing the unknown facts.

For every input x_i , the corresponding weight value w_i is multiplied indicating the strength of the connection. The one with a higher influence on the output value is triggered.

Fig. 4 Basic architecture of artificial neural network (ANN)



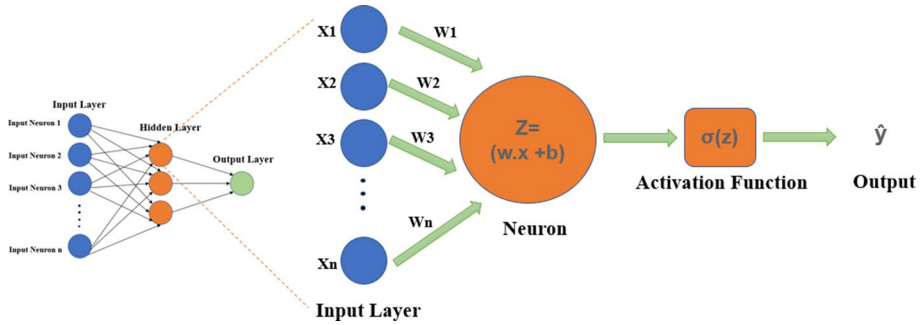


Fig. 5 Single-layer perceptron

$$\sum = (x_1 \times w_1) + (x_2 \times w_2) + \dots (x_n \times w_n) \tag{4}$$

where, $x = [x_1, x_2, x_3 \dots x_n]$ and $w = [w_1, w_2, w_3 \dots w_n]$ are the row vectors belonging to input and the weights respectively. Therefore, the dot product is given by:

$$x \cdot w = (x_1 \times w_1) + (x_2 \times w_2) + \dots (x_n \times w_n) \tag{5}$$

$$\sum = x \cdot w \tag{6}$$

Bias acts as an offset for the activation function and produces the output value.

$$z = x \cdot w + b \tag{7}$$

This intermediate value generated is passed to a non-linear activation function which governs the learning speed of the network. There exists a multitude of activation functions, depending upon the problem. One of the simplest ones is the sigmoid activation function, \hat{y} gives the predicted value and σ is the activation function, and it is computed as,

$$\hat{y} = \sigma(z) = \frac{1}{1 + e^{-z}} \tag{8}$$

The training mechanism includes back-propagating the error by computing the gradient values with respect to the weight. The mean square error is calculated by the difference between the actual values (y_i) and the predicted values (\hat{y}_i) of error,

$$MSI_i = (y_i - \hat{y}_i)^2 \tag{9}$$

The cumulative error for the entire training set is termed as loss function, which is calculated as,

$$MSE = \frac{1}{n} \sum_{i=1}^n (y_i - \hat{y}_i)^2 \tag{10}$$

Later, the weights can be optimized and hyper-parameters such as the minimum error, number of epochs, and learning rates can be fixed. A training: validation: testing ratio of 70:15:15 is used to measure the prediction accuracy of the ANN model.

Results and discussions

Variability in the measured leaf nitrogen concentration (LNC)

The LNC is one of the major indicators used to describe the leaf nitrogen status in different crops. Figure 6a shows the variation in LNC at different levels of nitrogen and water stresses. Figures 6b, c are the maps showing the nitrogen stress levels and LNC. As an observation, for every irrigation level, the LNC shows an increasing trend with a decrease in nitrogen stress. The average value of LNC corresponding to N_0 is 4.30% and for N_4 treatment is 5.28%. The LNC ranges from 4.19 to 5.12% in I_1 , 4.22 to 5.48% in I_2 , and 4.48 to 5.24% in I_3 irrigation treatments. No significant change was observed with varying levels of irrigation. A similar trend is detected for the wheat plant in the case of LNC at different water and nitrogen stresses for the tillering stage (Ranjan et al., 2012). At the recommended value of 150 kg ha^{-1} (N_3), the LNC shows a maximum value of 4.90% in I_1 and 4.69% in I_2 . When it comes to zero where no N application was done, the LNC varies between 4.19% in I_1 to 4.48% in I_3 . The variation in irrigation levels affects more on plant nitrogen accumulation (PNA) than LNC (Ranjan et al., 2012). The overall results of LNC indicate that the different N stress levels play an important role in the N status in the leaves of wheat plants.

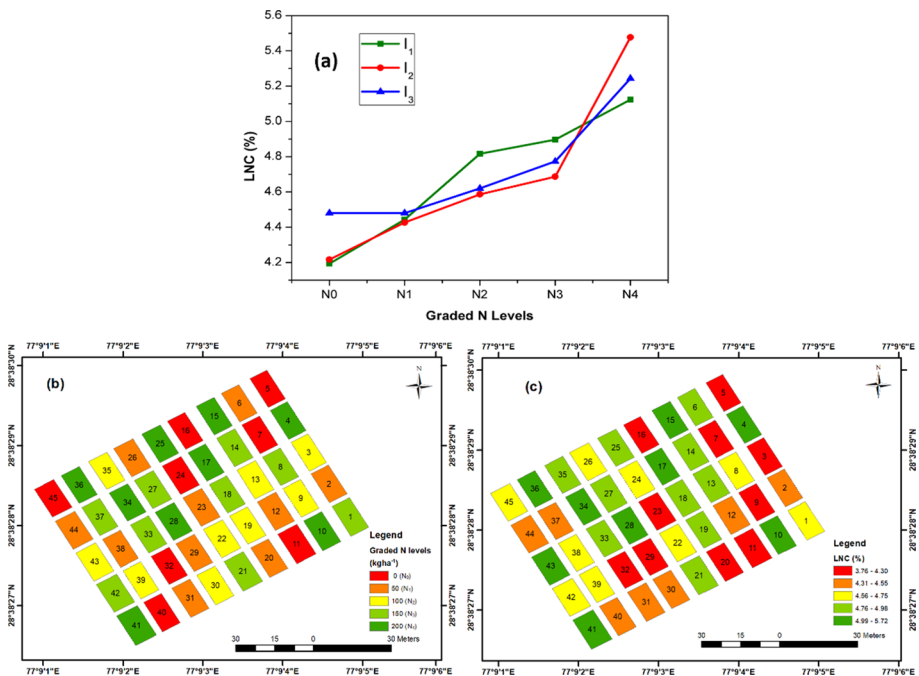


Fig. 6 a LNC variation at different levels of nitrogen and water stresses; b graded N levels; and c measured leaf nitrogen

Optimal indices for leaf N prediction

The pre-processed hyperspectral imagery of the wheat plots is shown in Fig. 7a. The wheat canopy area of the study site was successfully segmented using a combined approach of hNDVI threshold and SAM binary masks as expounded in the previous section. The crop area of 45 wheat plots is shown in Fig. 7b. These data were used for generating 61 vegetation indices for analyzing the plant N status using LNC.

All the indices summarized in Table 2 are sensitive to plant N and hold significance for predicting the LNC using the feature importance score. A large number of vegetation indices were used to explore the potential of optimizing feature variables combined with machine learning models for predicting N content. The graph showing the feature importance scores for all 61 vegetation indices derived from R^2 and VIP is shown in Fig. 8. The feature importance scores of R^2 and VIP help in ranking the 61 indices for selecting the best ones. The GMI1 performed the best with an R^2 score of 0.81 while the NPQI performed the least with a R^2 score of 0.01. In the case of VIP, the best index is MSAVI with a performance score of 0.72 and the lowest performance was shown by BNI.

The selection of important spectral variables for calculating VIF scores was done based on threshold criteria, $R^2 > 0.7$, and $VIP > 0.5$. On applying these thresholds, 39 and 15 indices were generated from R^2 and VIP respectively. Then the VIF technique was applied to these two sets of data for generating the optimal indices. The VIF generates 15 and 13 indices each from these two sets, out of which 13 were found to be common and they were selected as the most suitable indices for N prediction. The GI and TVI were excluded from the final list of suitable indices since they were only obtained from the VIP calculation. The VIF score of the 13 suitable indices is shown in Fig. 9.

Among the selected 61 indices, 13 indices showing the best correlation with measured leaf N are taken for Leaf N prediction. They are NDCI, GMI2, RI_half, PSSRa, SR_900, RI_1db, SR₇₀₅, Ctr1, RI_3db, RVI3, GMI1, ZM, and MSAVI. The selected indices belong to Red-edge spectral region (0.7 and 0.8 μm) which is found sensitive toward LNC (Raj, 2021). The spectral regions 350–710 nm and 740–1100 nm are equivalently considered highly sensitive to LNC at different N stresses (Ranjan et al., 2012). In literature, the N deficiency in corn canopies was successfully derived by an increase in red reflectance and a decrease in NIR reflectance (Walburg et al., 1981). The red (671 nm), NIR (780 nm) and the spectral region between 550 and 710 nm are relatively sensitive to plant N levels (Stone et al., 1996; Zhao et al., 2005). Since the visible

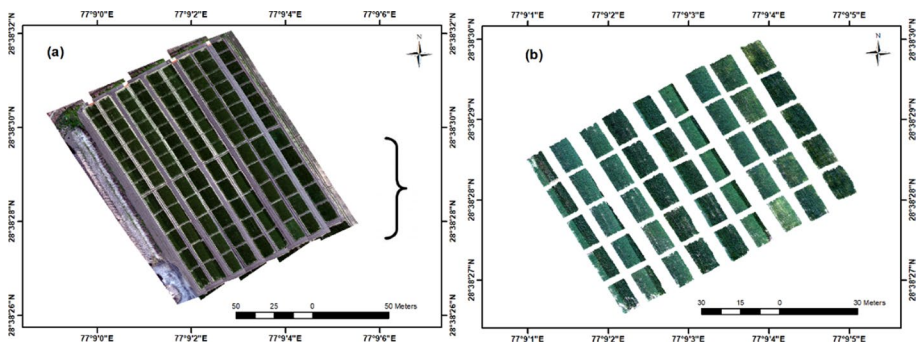


Fig. 7 a UAV hyperspectral imagery of the experimental plot; b masked vegetation

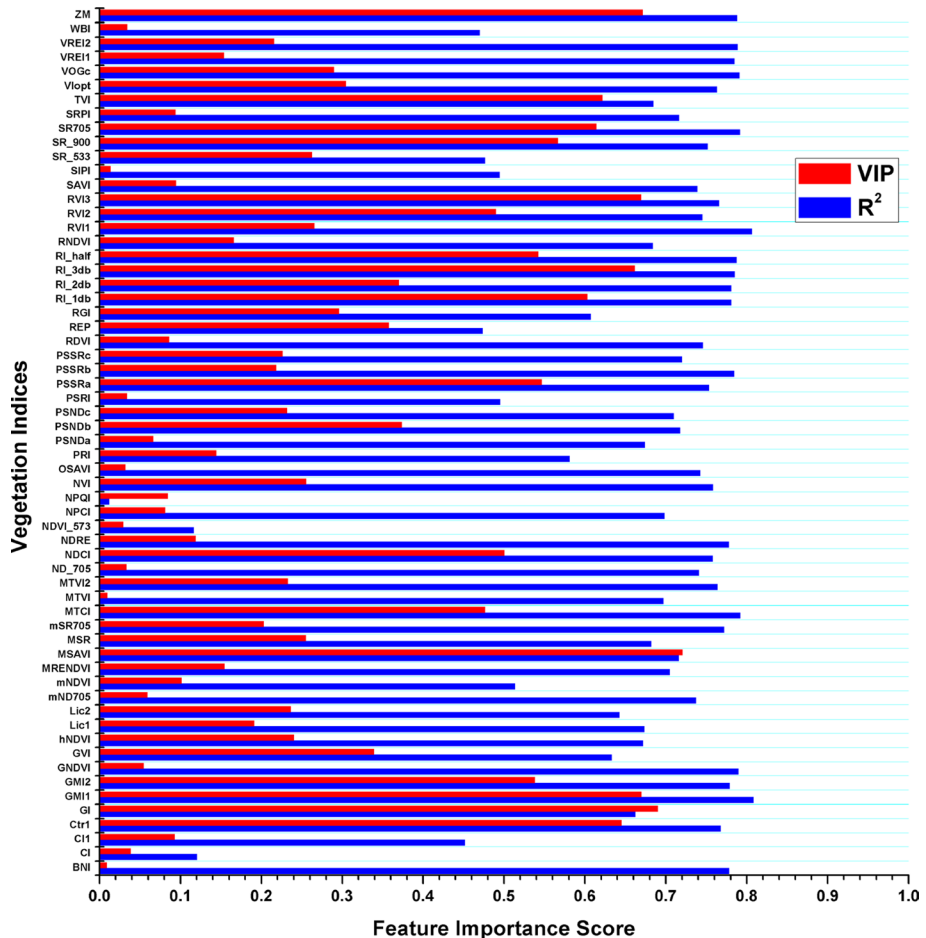


Fig. 8 Variable importance ranking for vegetation indices derived from R² and VIP

bands are strong absorbers of chlorophyll especially in red and blue regions (Hansen & Schjoerring 2003; Pablo J. Zarco-Tejada et al., 2001), the optimal indices generated from the present study contain bands from visible and red-edge regions thus proving the ability to evaluate crop growth and N status. The vegetation indices developed by selecting spectral bands from visible regions show strong absorption by chlorophyll and hence it proved to be very useful in predicting the nitrogen status in plants (Ranjan et al., 2012). The indices such as Ctr1, GMI-1, GMI-2, NDCI, SR₇₀₅, ZM and PSSRa are used for examining the Chlorophyll content in plants (Broge & Leblanc 2001; Gitelson & Merzlyak 1994). The RVI3 indicates the leaf nitrogen accumulation (Zhu et al., 2008). Further, MSAVI, RI-1dB, RI-3db, and RI-half are used for analyzing the vegetation sensitivity of plants. And finally, the indices such as SR₉₀₀ are used for measuring above-ground green biomass (Rouse et al., 1974). The N along with other macro-nutrients such as phosphorous (P) from soil are significant in the synthesis of chlorophyll during photosynthesis (Fredeen et al., 1990). So, N is one of the major constituents of chlorophyll which is closely associated with leaf color, crop yield, and growth (Fageria

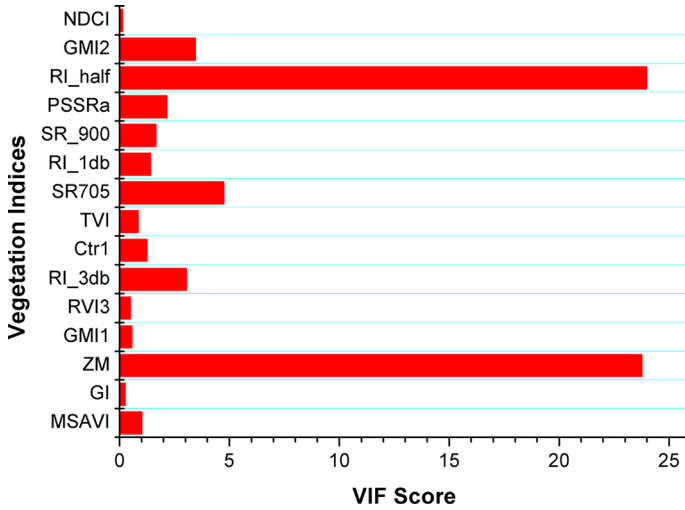


Fig. 9 Graph showing the VIF scores obtained for selected indices

et al., 2010). Thus it is demonstrated that the optimal indices selected from the present study show a strong relationship with the leaf N content in plants. Figure 10 and 11 show the maps of optimal vegetation indices and Table 3 summarizes the characteristics by which the suitable indices are influenced. The maximum and minimum values corresponding to each index are specifically seen in plots with N_4 and N_0 treatments. The R^2 score of these 13 indices ranges from 0.66 to 0.81, which implies that their index values are best correlated with LNC. The highest VIF score was shown by both ZM and RI_half while the least score was shown by NDCI.

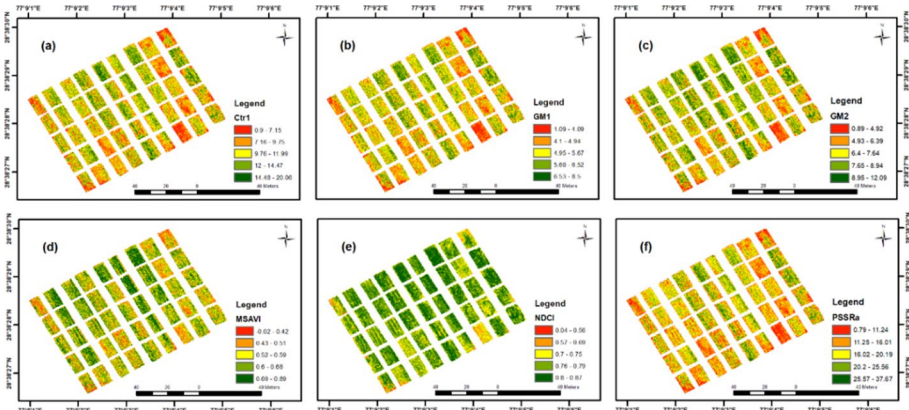


Fig. 10 Vegetative Indices generated using UAV hyperspectral image. a Ctr1; b GMI-1; c GMI-2; d MSAVI; e NDCI; f PSSRa

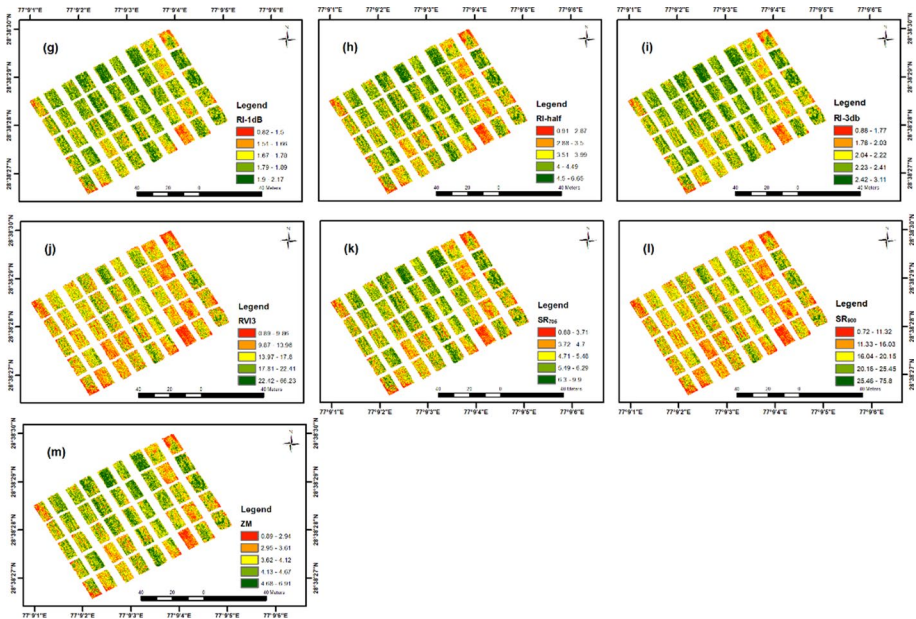


Fig. 11 Vegetative Indices generated using UAV hyperspectral image (Continued). **g** RI-1dB; **h** RI-half; **i** RI-3db; **j** RVI3; **k** SR₇₀₅; **l** SR₉₀₀; **m** ZM

Table 3 Categorisation of selected indices based on different plant characteristics

S. No.	Characteristics	Indices
1.	Chlorophyll content	Ctr1, GMI-1, GMI-2, NDCI, SR ₇₀₅ , ZM and PSSRa
2.	Vegetation sensitivity of plants	MSAVI, RI-1dB, RI-3db, and RI-half
3.	Above-ground green biomass	SR ₉₀₀

Leaf nitrogen prediction

ANN architecture with 13 input, 10 hidden neurons, and an output node has been constructed to train the network for the prediction of N content. The training: validation: testing ratio is 70:15:15 with an R-square value of 0.97, 0.84, and 0.86 respectively. The regression plots shown in Fig. 12 illustrate the network output plotted versus the targets as open circles. The best linear fit is indicated by a dashed line and the solid line represents the perfect fit.

Further, the best validation performance is obtained at 0.067 mean square error (MSE) at 5 epochs. The result seems reasonable as the test set error and the validation set error have similar characteristics therefore any significant overfitting has not occurred [Refer to Fig. 13a]. The error histogram is plotted between the observed and predicted N values, after training the neural network, where the y-axis represents the number of samples in a particular bin, as shown in Fig. 13b. From Fig. 13c, the final value of the gradient coefficient at epoch number 11 is 0.0114 approximated with minimum error, also the gradient

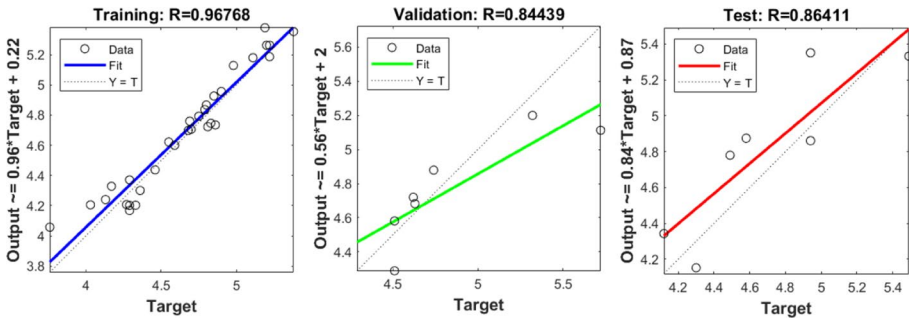


Fig. 12 Regression plots for N prediction using ANN

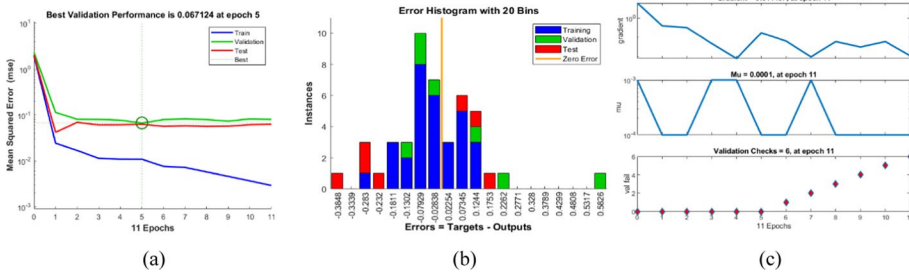


Fig. 13 Performance evaluation using ANN for N prediction. **a** Best validation performance, **b** error histogram, **c** training set histogram

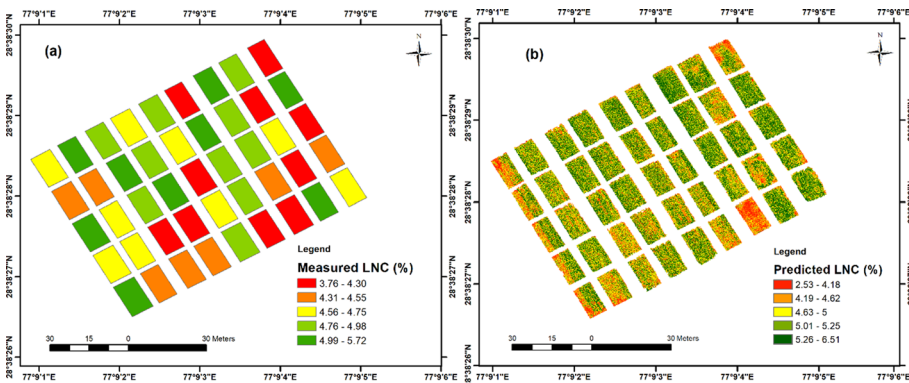


Fig. 14 Leaf N prediction using ANN. **a** Measured LNC; **b** Predicted LNC

value keeps on decreasing with increasing the epoch. The N-predicted map generated using the ANN is shown in Fig. 14. The predicted LNC ranges from 2.53 to 6.51%. The current approach of N prediction significantly reduces the salt and pepper noise pertaining to the raw image. The noise is still observed in the overlapping regions due to the averaging of pixel values during ortho-mosaicking. Also, less salt and pepper noise and misclassification were reported for random forest (RF) (Wang et al., 2021) and deep convolutional neural network (CNN) classification (Zhong et al., 2020) of UAV data. This method presented

is an alternate approach for the UAV-based imaging spectroscopy for predicting wheat leaf nitrogen using spectral modelling technique (Sahoo et al., 2023).

Conclusion

Leaf N assessment for the winter wheat crop concerning different nitrogen levels was successfully evaluated for the considered experimental field. A UAV-based hyperspectral push-broom scanner system seems to be capable of acquiring high-resolution spatial and spectral data for N studies in precision farming. However, the side overlap regions after mosaicking the scanlines is still an area of concern but later be tackled for the prediction of N values. The hyperspectral imagery of ultra-high spatial resolution was captured over the experimental wheat fields under varying irrigation and nitrogen treatments. After pre-processing and removal of spectral noises, the crop area is extracted for prediction of N values to avoid the intervening effect of other features such as impervious areas, soil, etc. Abrupt increase or decrease in reflectance values has been observed in the overlapping areas in multiple scan lines to generate the mosaiced image, which is decreased using ANN as a prediction model. About 61 vegetative indices have been computed, out of which 13 most suitable indices were extracted using a combined approach of R-Square and VIP followed by the VIF technique. These optimal indices were used in the ANN model for the prediction of leaf N values for the entire field. The prediction model shows an R-square value of 0.97, 0.84, and 0.86 for training, validation, and testing respectively, suggesting high prediction accuracy. The generated N map seems to be similar to the ground-truth values of N produced for every plot making the proposed approach viable for the same. The approach seems to be fast, accurate, and suitable for N prediction, further, it may be upscaled for the farmer's field level with the availability of field data. The generated spatial map may be used by a sprayer drone for site-specific nitrogen application to promote sustainability and economical use. A similar technique may be deployed for other crop-related parameters, such as chlorophyll and leaf area index (LAI), etc. as well.

Acknowledgement This research activity was conducted under financial support of the Indian Council of Agricultural Research (ICAR) and is hereby duly acknowledged under the project, titled 'Network Program on Precision Agriculture (NePPA)'.

Declarations

Conflict of interest The authors have declared no conflict of interest.

References

- Adak, S., Bandyopadhyay, K. K., Sahoo, R. N., Mridha, N., Shrivastava, M., & Purakayastha, T. J. (2021). Prediction of wheat yield using spectral reflectance indices under different tillage, residue and nitrogen management practices. *Current Science*. <https://doi.org/10.18520/cs/v121/i3/402-413>
- Ågren, G. I., Wetterstedt, J. Å. M., & Billberger, M. F. K. (2012). Nutrient limitation on terrestrial plant growth - modeling the interaction between nitrogen and phosphorus. *New Phytologist*. <https://doi.org/10.1111/j.1469-8137.2012.04116.x>
- Anderegg, J., Tschurr, F., Kirchgessner, N., Treier, S., Schmucki, M., Streit, B., & Walter, A. (2023). On-farm evaluation of UAV-based aerial imagery for season-long weed monitoring under contrasting management and pedoclimatic conditions in wheat. *Computers and Electronics in Agriculture*. <https://doi.org/10.1016/j.compag.2022.107558>

- Baresel, J. P., Zimmermann, G., & Reents, H. J. (2008). Effects of genotype and environment on N uptake and N partition in organically grown winter wheat (*Triticum aestivum* L.) in Germany. *Euphytica*. <https://doi.org/10.1007/s10681-008-9718-1>
- Barnes, J. D., Balaguer, L., Manrique, E., Elvira, S., & Davison, A. W. (1992). A reappraisal of the use of DMSO for the extraction and determination of chlorophylls a and b in lichens and higher plants. *Environmental and Experimental Botany*. [https://doi.org/10.1016/0098-8472\(92\)90034-Y](https://doi.org/10.1016/0098-8472(92)90034-Y)
- Basyouni, R., Dunn, B. L., & Goad, C. (2015). Use of nondestructive sensors to assess nitrogen status in potted poinsettia (*Euphorbia pulcherrima* L. (Willd. ex Klotzsch)) production. *Scientia Horticulturae*. <https://doi.org/10.1016/j.scienta.2015.05.011>
- Blackburn, G. A. (1998). Spectral indices for estimating photosynthetic pigment concentrations: A test using senescent tree leaves. *International Journal of Remote Sensing*. <https://doi.org/10.1080/014311698215919>
- Blekanov, I., Molin, A., Zhang, D., Mitrofanov, E., Mitrofanova, O., & Li, Y. (2023). Monitoring of grain crops nitrogen status from uav multispectral images coupled with deep learning approaches. *Computers and Electronics in Agriculture*. <https://doi.org/10.1016/j.compag.2023.108047>
- Broge, N. H., & Leblanc, E. (2001). Comparing prediction power and stability of broadband and hyperspectral vegetation indices for estimation of green leaf area index and canopy chlorophyll density. *Remote Sensing of Environment*. [https://doi.org/10.1016/S0034-4257\(00\)00197-8](https://doi.org/10.1016/S0034-4257(00)00197-8)
- Buschmann, C., & Nagel, E. (1993). In vivo spectroscopy and internal optics of leaves as basis for remote sensing of vegetation. *International Journal of Remote Sensing*. <https://doi.org/10.1080/01431169308904370>
- Buthelezi, S., Mutanga, O., Sibanda, M., Odindi, J., Clulow, A. D., Chimonyo, V. G. P., & Mabhaudhi, T. (2023). Assessing the prospects of remote sensing maize leaf area index using UAV-derived multi-spectral data in smallholder farms across the growing season. *Remote Sensing*. <https://doi.org/10.3390/rs15061597>
- Carter, G. A. (1994). Ratios of leaf reflectances in narrow wavebands as indicators of plant stress. *International Journal of Remote Sensing*. <https://doi.org/10.1080/01431169408954109>
- Chandel, N. S., Tiwari, P. S., Singh, K. P., Jat, D., Gaikwad, B. B., Tripathi, H., & Golhani, K. (2019). Yield prediction in wheat (*Triticum aestivum* L.) using spectral reflectance indices. *Current Science*. <https://doi.org/10.18520/cs/v116/i2/272-278>
- Chen, J. M. (1996). Evaluation of vegetation indices and a modified simple ratio for boreal applications. *Canadian Journal of Remote Sensing*. <https://doi.org/10.1080/07038992.1996.10855178>
- Dash, J., & Curran, P. J. (2004). The MERIS terrestrial chlorophyll index. *International Journal of Remote Sensing*. <https://doi.org/10.1080/0143116042000274015>
- Datt, B. (1999). Visible/near infrared reflectance and chlorophyll content in eucalyptus leaves. *International Journal of Remote Sensing*. <https://doi.org/10.1080/014311699211778>
- Datt, B. (1999). A new reflectance index for remote sensing of chlorophyll content in higher plants: Tests using Eucalyptus leaves. *Journal of Plant Physiology*. [https://doi.org/10.1016/S0176-1617\(99\)80314-9](https://doi.org/10.1016/S0176-1617(99)80314-9)
- Dehghan-Shoar, M. H., Orsi, A. A., Pullanagari, R. R., & Yule, I. J. (2023). A hybrid model to predict nitrogen concentration in heterogeneous grassland using field spectroscopy. *Remote Sensing of Environment*. <https://doi.org/10.1016/j.rse.2022.113385>
- Esposito, M., Crimaldi, M., Cirillo, V., Sarghini, F., & Maggio, A. (2021). Drone and sensor technology for sustainable weed management: a review. *Chemical and Biological Technologies in Agriculture*. <https://doi.org/10.1186/s40538-021-00217-8>
- Fageria, N. K., Baligar, V. C., & Jones, C. A. (2010). *Growth and mineral nutrition of field crops, third edition. Growth and Mineral Nutrition of Field Crops* (3rd ed.). CRC Press. <https://doi.org/10.1201/b10160>
- Fredeen, A. L., Raab, T. K., Rao, I. M., & Terry, N. (1990). Effects of phosphorus nutrition on photosynthesis in *Glycine max* (L.) Merr. *Planta*. <https://doi.org/10.1007/BF00195894>
- Fu, Z., Yu, S., Zhang, J., Xi, H., Gao, Y., Lu, R., et al., (2022). Combining UAV multispectral imagery and ecological factors to estimate leaf nitrogen and grain protein content of wheat. *European Journal of Agronomy*. <https://doi.org/10.1016/j.eja.2021.126405>
- Garbulsky, M. F., Peñuelas, J., Gamon, J., Inoue, Y., & Filella, I. (2011). The photochemical reflectance index (PRI) and the remote sensing of leaf, canopy and ecosystem radiation use efficiencies. A review and meta-analysis. *Remote Sensing of Environment*. <https://doi.org/10.1016/j.rse.2010.08.023>
- Ge, X., Wang, J., Ding, J., Cao, X., Zhang, Z., Liu, J., & Li, X. (2019). Combining UAV-based hyperspectral imagery and machine learning algorithms for soil moisture content monitoring. *PeerJ*. <https://doi.org/10.7717/peerj.6926>

- Gitelson, A. A., Kaufman, Y. J., & Merzlyak, M. N. (1996). Use of a green channel in remote sensing of global vegetation from EOS-MODIS. *Remote Sensing of Environment*. [https://doi.org/10.1016/S0034-4257\(96\)00072-7](https://doi.org/10.1016/S0034-4257(96)00072-7)
- Gitelson, A. A., & Merzlyak, M. N. (1998). Remote sensing of chlorophyll concentration in higher plant leaves. *Advances in Space Research*. [https://doi.org/10.1016/S0273-1177\(97\)01133-2](https://doi.org/10.1016/S0273-1177(97)01133-2)
- Gitelson, A., & Merzlyak, M. N. (1994). Spectral reflectance changes associated with autumn senescence of *Aesculus hippocastanum* L. and *Acer platanoides* L. leaves. Spectral features and relation to chlorophyll estimation. *Journal of Plant Physiology*. [https://doi.org/10.1016/S0176-1617\(11\)81633-0](https://doi.org/10.1016/S0176-1617(11)81633-0)
- Good, A. G., & Beatty, P. H. (2011). Fertilizing nature: A tragedy of excess in the commons. *PLoS Biology*. <https://doi.org/10.1371/journal.pbio.1001124>
- Guebel, D. V., Nudel, B. C., & Giulietti, A. M. (1991). A simple and rapid micro-Kjeldahl method for total nitrogen analysis. *Biotechnology Techniques*. <https://doi.org/10.1007/BF00155487>
- Guo, J., Jia, Y., Chen, H., Zhang, L., Yang, J., Zhang, J., et al., (2019). Growth, photosynthesis, and nutrient uptake in wheat are affected by differences in nitrogen levels and forms and potassium supply. *Scientific Reports*. <https://doi.org/10.1038/s41598-018-37838-3>
- Gupta, R. K., Vijayan, D., & Prasad, T. S. (2001). New hyperspectral vegetation characterization parameters. *Advances in Space Research*. [https://doi.org/10.1016/S0273-1177\(01\)00346-5](https://doi.org/10.1016/S0273-1177(01)00346-5)
- Gupta, R. K., Vijayan, D., & Prasad, T. S. (2003). Comparative analysis of red-edge hyperspectral indices. *Advances in Space Research*. [https://doi.org/10.1016/S0273-1177\(03\)90545-X](https://doi.org/10.1016/S0273-1177(03)90545-X)
- Guyot, G., & Baret, F. (1988). Utilisation de la haute resolution spectrale pour suivre l'état des couverts végétaux. *Journal of Chemical Information and Modeling*, 53(9), 279.
- Haboudane, D., Miller, J. R., Pattey, E., Zarco-Tejada, P. J., & Strachan, I. B. (2004). Hyperspectral vegetation indices and novel algorithms for predicting green LAI of crop canopies: Modeling and validation in the context of precision agriculture. *Remote Sensing of Environment*. <https://doi.org/10.1016/j.rse.2003.12.013>
- Hansen, P. M., & Schjoerring, J. K. (2003). Reflectance measurement of canopy biomass and nitrogen status in wheat crops using normalized difference vegetation indices and partial least squares regression. *Remote Sensing of Environment*. [https://doi.org/10.1016/S0034-4257\(03\)00131-7](https://doi.org/10.1016/S0034-4257(03)00131-7)
- Haque, T. (2006). Resource use efficiency in Indian agriculture. *Indian Journal of Agricultural Economics*, 61, 66.
- Hirel, B., Tétu, T., Lea, P. J., & Dubois, F. (2011). Improving nitrogen use efficiency in crops for sustainable agriculture. *Sustainability*. <https://doi.org/10.3390/su3091452>
- Hunt, E. R., Cavigelli, M., Daughtry, C. S. T., McMurtrey, J. E., & Walthall, C. L. (2005). Evaluation of digital photography from model aircraft for remote sensing of crop biomass and nitrogen status. *Precision Agriculture*. <https://doi.org/10.1007/s11119-005-2324-5>
- Jamali, M., Soufizadeh, S., Yeganeh, B., & Emam, Y. (2023). Wheat leaf traits monitoring based on machine learning algorithms and high-resolution satellite imagery. *Ecological Informatics*. <https://doi.org/10.1016/j.ecoinf.2022.101967>
- Jiang, J., Cai, W., Zheng, H., Cheng, T., Tian, Y., Zhu, Y., et al., (2019). Using digital cameras on an unmanned aerial vehicle to derive optimum color vegetation indices for leaf nitrogen concentration monitoring in winter wheat. *Remote Sensing*. <https://doi.org/10.3390/rs11222667>
- Jiang, J., Atkinson, P. M., Chen, C., Cao, Q., Tian, Y., Zhu, Y., et al. (2023). Combining UAV and Sentinel-2 satellite multi-spectral images to diagnose crop growth and N status in winter wheat at the county scale. *Field Crops Research*. <https://doi.org/10.1016/j.fcr.2023.108860>
- Jiang, J., Wang, C., Wang, Y., Cao, Q., Tian, Y., Zhu, Y., et al. (2020). Using an active sensor to develop new critical nitrogen dilution curve for winter wheat. *Sensors (Switzerland)*. <https://doi.org/10.3390/s20061577>
- Jurado-Expósito, M., Torres-Sánchez, J., López-Granados, F., & Jiménez-Brenes, F. M. (2021). Monitoring the spatial variability of knapweed (*Centaurea diluta* aiton) in wheat crops using geostatistics and uav imagery: Probability maps for risk assessment in site-specific control. *Agronomy*. <https://doi.org/10.3390/agronomy11050880>
- Kauth, R. J., & Thomas, G. S. (1976). The tasselled cap—a graphic description of the spectral-temporal development of agricultural crops as seen by Landsat. In LARS symposia, p. 159.
- Li, S., Ding, X., Kuang, Q., Ata-UI-Karim, S. T., Cheng, T., & Liu, X. (2018). Potential of UAV-based active sensing for monitoring rice leaf nitrogen status. *Frontiers in Plant Science*. <https://doi.org/10.3389/fpls.2018.01834>
- Liang, L., Di, L., Huang, T., Wang, J., Lin, L., Wang, L., & Yang, M. (2018). Estimation of leaf nitrogen content in wheat using new hyperspectral indices and a random forest regression algorithm. *Remote Sensing*. <https://doi.org/10.3390/rs10121940>

- Lichtenthaler, H. K., Gitelson, A., & Lang, M. (1996). Non-destructive determination of chlorophyll content of leaves of a green and an aurea mutant of tobacco by reflectance measurements. *Journal of Plant Physiology*. [https://doi.org/10.1016/S0176-1617\(96\)80283-5](https://doi.org/10.1016/S0176-1617(96)80283-5)
- Liu, H., Zhu, H., & Wang, P. (2017). Quantitative modelling for leaf nitrogen content of winter wheat using UAV-based hyperspectral data. *International Journal of Remote Sensing*, 38, 8–10. <https://doi.org/10.1080/01431161.2016.1253899>.
- Lu, N., Wang, W., Zhang, Q., Li, D., Yao, X., Tian, Y., et al. (2019). Estimation of nitrogen nutrition status in winter wheat from unmanned aerial vehicle based multi-angular multispectral imagery. *Frontiers in Plant Science*. <https://doi.org/10.3389/fpls.2019.01601>
- Mălinaș, A., Vidican, R., Rotar, I., Mălinaș, C., Moldovan, C. M., & Proorocu, M. (2022). Current status and future prospective for nitrogen use efficiency in wheat (*Triticum aestivum* L). *Plants*. <https://doi.org/10.3390/plants11020217>
- Maresma, A., Ariza, M., Martínez, E., Lloveras, J., & Martínez-Casasnovas, J. A. (2016). Analysis of vegetation indices to determine nitrogen application and yield prediction in maize (*Zea mays* L.) from a standard uav service. *Remote Sensing*. <https://doi.org/10.3390/rs8120973>
- Marshak, A., Knyazikhin, Y., Davis, A. B., Wiscombe, W. J., & Pilewskie, P. (2000). Cloud - vegetation interaction: Use of normalized difference cloud index for estimation of cloud optical thickness. *Geophysical Research Letters*. <https://doi.org/10.1029/1999GL010993>
- Merzlyak, M. N., Gitelson, A. A., Chivkunova, O. B., & Rakitin, V. Y. (1999). Non-destructive optical detection of pigment changes during leaf senescence and fruit ripening. *Physiologia Plantarum*. <https://doi.org/10.1034/j.1399-3054.1999.106119.x>
- Oscó, L. P., Junior, J. M., Ramos, A. P. M., Furuya, D. E. G., Santana, D. C., Teodoro, L. P. R., et al. (2020). Leaf nitrogen concentration and plant height prediction for maize using UAV-based multispectral imagery and machine learning techniques. *Remote Sensing*. <https://doi.org/10.3390/rs12193237>
- Penuelas, J., Baret, F., & Filella, I. (1995). Semi-empirical indices to assess carotenoids/chlorophyll a ratio from leaf spectral reflectance. *Photosynthetica*, 31(2), 221.
- Penuelas, J., Filella, I., Biel, C., Serrano, L., & Save, R. (1993). The reflectance at the 950–970 nm region as an indicator of plant water status. *International Journal of Remote Sensing*. <https://doi.org/10.1080/01431169308954010>
- Peñuelas, J., Gamon, J. A., Fredeen, A. L., Merino, J., & Field, C. B. (1994). Reflectance indices associated with physiological changes in nitrogen- and water-limited sunflower leaves. *Remote Sensing of Environment*. [https://doi.org/10.1016/0034-4257\(94\)90136-8](https://doi.org/10.1016/0034-4257(94)90136-8)
- Pradhan, S., Bandyopadhyay, K. K., Sahoo, R. N., Sehgal, V. K., Singh, R., Joshi, D. K., & Gupta, V. K. (2013). Prediction of wheat (*Triticum aestivum*) grain and biomass yield under different irrigation and nitrogen management practices using canopy reflectance spectra model. *Indian Journal of Agricultural Sciences*, 83(11), 1136.
- Qi, J., Chehbouni, A., Huete, A. R., Kerr, Y. H., & Sorooshian, S. (1994). A modified soil adjusted vegetation index. *Remote Sensing of Environment*. [https://doi.org/10.1016/0034-4257\(94\)90134-1](https://doi.org/10.1016/0034-4257(94)90134-1)
- Rabatel, G., Al Makdessi, N., Ecartot, M., & Roumet, P. (2017). A spectral correction method for multi-scatterer effects in close range hyperspectral imagery of vegetation scenes: application to nitrogen content assessment in wheat. *Advances in Animal Biosciences*. <https://doi.org/10.1017/s2040470017000164>
- Raj, R. (2021). Drone-based sensing for identification of at-risk water and nitrogen stress areas for on-farm management. PhD Dissertation, IITB-Monash Research Academy.
- Ranjan, R., Chopra, U. K., Sahoo, R. N., Singh, A. K., & Pradhan, S. (2012). Assessment of plant nitrogen stress in wheat (*Triticum aestivum* L.) through hyperspectral indices. *International Journal of Remote Sensing*. <https://doi.org/10.1080/01431161.2012.687473>
- Raun, W. R., Solie, J. B., Johnson, G. V., Stone, M. L., Lukina, E. V., Thomason, W. E., & Schepers, J. S. (2001). In-season prediction of potential grain yield in winter wheat using canopy reflectance. *Agronomy Journal*. <https://doi.org/10.2134/agronj2001.931131x>
- Rejith, R. G., Sundararajan, M., Gnanappazham, L., & Loveson, V. J. (2020). Satellite-based spectral mapping (ASTER and landsat data) of mineralogical signatures of beach sediments: a precursor insight. *Geocarto International*. <https://doi.org/10.1080/10106049.2020.1750061>
- Rodriguez, D., Fitzgerald, G. J., Belford, R., & Christensen, L. K. (2006). Detection of nitrogen deficiency in wheat from spectral reflectance indices and basic crop eco-physiological concepts. *Australian Journal of Agricultural Research*. <https://doi.org/10.1071/AR05361>
- Rondeaux, G., Steven, M., & Baret, F. (1996). Optimization of soil-adjusted vegetation indices. *Remote Sensing of Environment*. [https://doi.org/10.1016/0034-4257\(95\)00186-7](https://doi.org/10.1016/0034-4257(95)00186-7)
- Roujean, J. L., & Breon, F. M. (1995). Estimating PAR absorbed by vegetation from bidirectional reflectance measurements. *Remote Sensing of Environment*. [https://doi.org/10.1016/0034-4257\(94\)00114-3](https://doi.org/10.1016/0034-4257(94)00114-3)

- Rouse, J. W., Haas, R. H., Schell, J. A., & Deering, D. W. (1974). Monitoring vegetation systems in the Great Plains with ERTS. *NASA special publication. NASA special publication*, 24(1), 309.
- Rouse, J. W., Hass, R. H., Schell, J. A., Deering, D. W., & Harlan, J. C. (1974). *Monitoring the vernal advancement and retrogradation (green wave effect) of natural vegetation*. Final Report, RSC 1978-4, Texas A & M University, College Station.
- Sahoo, R. N., Ray, S. S., & Manjunath, K. R. (2015). Hyperspectral remote sensing of agriculture. *Current Science*, 108(5), 848.
- Sahoo, R. N., Gakhar, S., Rejith, R. G., Ranjan, R., Meena, M. C., Dey, A., et al. (2023). Unmanned Aerial Vehicle (UAV)-Based Imaging Spectroscopy for Predicting Wheat Leaf Nitrogen. *Photogrammetric Engineering & Remote Sensing*. <https://doi.org/10.14358/pers.22-00089r2>
- Santos-Rufo, A., Mesas-Carrascosa, F. J., García-Ferrer, A., & Meroño-Larriva, J. E. (2020). Wavelength selection method based on partial least square from hyperspectral unmanned aerial vehicle orthomosaic of irrigated olive orchards. *Remote Sensing*. <https://doi.org/10.3390/rs12203426>
- Sims, D. A., & Gamon, J. A. (2002). Relationships between leaf pigment content and spectral reflectance across a wide range of species, leaf structures and developmental stages. *Remote Sensing of Environment*. [https://doi.org/10.1016/S0034-4257\(02\)00010-X](https://doi.org/10.1016/S0034-4257(02)00010-X)
- Späti, K., Huber, R., & Finger, R. (2021). Benefits of increasing information accuracy in variable rate technologies. *Ecological Economics*. <https://doi.org/10.1016/j.ecolecon.2021.107047>
- Stone, M. L., Solie, J. B., Raun, W. R., Whitney, R. W., Taylor, S. L., & Ringer, J. D. (1996). Use of spectral radiance for correcting in-season fertilizer nitrogen deficiencies in winter wheat. *Transactions of the American Society of Agricultural Engineers*. <https://doi.org/10.13031/2013.27678>
- Tian, Y. C., Yao, X., Yang, J., Cao, W. X., Hannaway, D. B., & Zhu, Y. (2011). Assessing newly developed and published vegetation indices for estimating rice leaf nitrogen concentration with ground- and space-based hyperspectral reflectance. *Field Crops Research*. <https://doi.org/10.1016/j.fcr.2010.11.002>
- UgCS (2017). <https://www.ugcs.com/>.
- Vogelmann, J. E., Rock, B. N., & Moss, D. M. (1993). Red edge spectral measurements from sugar maple leaves. *International Journal of Remote Sensing*. <https://doi.org/10.1080/01431169308953986>
- Walburg, G., Bauer, M. E., & Daughtry, C. S. T. (1981). *Effects of nitrogen nutrition on the growth, yield and reflectance characteristics of corn canopies*. Purdue University, LARS Technical Report, 030381. <https://doi.org/10.2134/agronj1982.00021962007400040020x>.
- Wang, L., Chen, S., Li, D., Wang, C., Jiang, H., Zheng, Q., & Peng, Z. (2021). Estimation of paddy rice nitrogen content and accumulation both at leaf and plant levels from uav hyperspectral imagery. *Remote Sensing*. <https://doi.org/10.3390/rs13152956>
- Wang, X., Wang, Y., Zhou, C., Yin, L., & Feng, X. (2021). Urban forest monitoring based on multiple features at the single tree scale by UAV. *Urban Forestry and Urban Greening*. <https://doi.org/10.1016/j.ufug.2020.126958>
- Xu, S., Xu, X., Blacker, C., Gaulton, R., Zhu, Q., Yang, M., et al. (2023). Estimation of leaf nitrogen content in rice using vegetation indices and feature variable optimization with information fusion of multiple-sensor images from UAV. *Remote Sensing*. <https://doi.org/10.3390/rs15030854>
- Xu, S., Xu, X., Zhu, Q., Meng, Y., Yang, G., Feng, H., et al. (2023). Monitoring leaf nitrogen content in rice based on information fusion of multi-sensor imagery from UAV. *Precision Agriculture*. <https://doi.org/10.1007/s11119-023-10042-8>.
- Xue, L., Cao, W., Luo, W., Dai, T., & Zhu, Y. (2004). Monitoring leaf nitrogen status in rice with canopy spectral reflectance. *Agronomy Journal*. <https://doi.org/10.2134/agronj2004.0135>
- Yang, B., Wang, M., Sha, Z., Wang, B., Chen, J., Yao, X., et al. (2019). Evaluation of aboveground nitrogen content of winter wheat using digital imagery of unmanned aerial vehicles. *Sensors (Switzerland)*. <https://doi.org/10.3390/s19204416>
- Zarco-Tejada, P. J., Berjón, A., López-Lozano, R., Miller, J. R., Martín, P., Cachorro, V., et al. (2005). Assessing vineyard condition with hyperspectral indices: Leaf and canopy reflectance simulation in a row-structured discontinuous canopy. *Remote Sensing of Environment*. <https://doi.org/10.1016/j.rse.2005.09.002>
- Zarco-Tejada, P. J., Miller, J. R., Noland, T. L., Mohammed, G. H., & Sampson, P. H. (2001). Scaling-up and model inversion methods with narrowband optical indices for chlorophyll content estimation in closed forest canopies with hyperspectral data. *IEEE Transactions on Geoscience and Remote Sensing*, 39(7), 1491–1507. <https://doi.org/10.1109/36.934080>.
- Zhang, J., Cheng, T., Shi, L., Wang, W., Niu, Z., Guo, W., & Ma, X. (2022). Combining spectral and texture features of UAV hyperspectral images for leaf nitrogen content monitoring in winter wheat. *International Journal of Remote Sensing*. <https://doi.org/10.1080/01431161.2021.2019847>

- Zhao, D., Reddy, K. R., Kakani, V. G., & Reddy, V. R. (2005). Nitrogen deficiency effects on plant growth, leaf photosynthesis, and hyperspectral reflectance properties of sorghum. *European Journal of Agronomy*. <https://doi.org/10.1016/j.eja.2004.06.005>
- Zheng, H., Li, W., Jiang, J., Liu, Y., Cheng, T., Tian, Y., et al. (2018). A comparative assessment of different modeling algorithms for estimating leaf nitrogen content in winter wheat using multispectral images from an unmanned aerial vehicle. *Remote Sensing*. <https://doi.org/10.3390/rs10122026>
- Zhong, Y., Hu, X., Luo, C., Wang, X., Zhao, J., & Zhang, L. (2020). WHU-Hi: UAV-borne hyperspectral with high spatial resolution (H2) benchmark datasets and classifier for precise crop identification based on deep convolutional neural network with CRF. *Remote Sensing of Environment*. <https://doi.org/10.1016/j.rse.2020.112012>
- Zhu, Y., Tian, Y., Yao, X., Liu, X., & Cao, W. (2007). Analysis of common canopy reflectance spectra for indicating leaf nitrogen concentrations in wheat and rice. *Plant Production Science*. <https://doi.org/10.1626/pp.s.10.400>
- Zhu, Y., Yao, X., Tian, Y. C., Liu, X. J., & Cao, W. X. (2008). Analysis of common canopy vegetation indices for indicating leaf nitrogen accumulations in wheat and rice. *International Journal of Applied Earth Observation and Geoinformation*. <https://doi.org/10.1016/j.jag.2007.02.006>

Publisher's Note Springer Nature remains neutral with regard to jurisdictional claims in published maps and institutional affiliations.

Springer Nature or its licensor (e.g. a society or other partner) holds exclusive rights to this article under a publishing agreement with the author(s) or other rightsholder(s); author self-archiving of the accepted manuscript version of this article is solely governed by the terms of such publishing agreement and applicable law.

Authors and Affiliations

Rabi N. Sahoo¹ · R. G. Rejith¹ · Shalini Gakhar¹ · Rajeev Ranjan¹ · Mahesh C. Meena² · Abir Dey² · Joydeep Mukherjee¹ · Rajkumar Dhakar¹ · Abhishek Meena¹ · Anchal Daas³ · Subhash Babu³ · Pravin K. Upadhyay³ · Kapila Sekhawat³ · Sudhir Kumar⁴ · Mahesh Kumar⁴ · Viswanathan Chinnusamy⁴ · Manoj Khanna⁵

✉ Rabi N. Sahoo
rabi.sahoo@icar.gov.in

R. G. Rejith
rejithrg01@gmail.com

Shalini Gakhar
shalinigakhar7@gmail.com

Rajeev Ranjan
rajeev.ranjan@icar.gov.in

Mahesh C. Meena
mcmeena@gmail.com

Abir Dey
drabiriari@gmail.com

Joydeep Mukherjee
joydeep.icar@gmail.com

Rajkumar Dhakar
rajdhakar.iari@gmail.com

Abhishek Meena
abhishek.meena1@icar.gov.in

Anchal Daas
anchal_iari@rediffmail.com

Subhash Babu
subhiari@gmail.com

Pravin K. Upadhyay
pravin.ndu@gmail.com

Kapila Sekhawat
drrathorekapila@gmail.com

Sudhir Kumar
sudhirnp2@gmail.com

Mahesh Kumar
mahesagrawal@gmail.com

Viswanathan Chinnusamy
viswa.chinnusamy@gmail.com

Manoj Khanna
khanna_manoj2001@yahoo.com.au

- ¹ Division of Agricultural Physics, ICAR - Indian Agricultural Research Institute (IARI), 110012 New Delhi, India
- ² Division of Soil Science & Agricultural Chemistry, ICAR-IARI, 110012 New Delhi, India
- ³ Division of Agronomy, ICAR-IARI, 110012 New Delhi, India
- ⁴ Division of Plant Physiology, ICAR-IARI, 110012 New Delhi, India
- ⁵ Water Technology Centre, ICAR-IARI, 110012 New Delhi, India